SIMULATION OF PHYSICAL PROCESSES

Original article
DOI: https://doi.org/10.18721/JPM.19202

STUDY OF VORTEX FLOWS GENERATED BY A PULSED TURBULENT BUOYANT JET

K. K. Ermakova, M. A. Zasimova, N. G. Ivanov✉

Peter the Great St. Petersburg Polytechnic University, St. Petersburg, Russia

✉ ivanov_ng@spbstu.ru

Abstract. In the paper, the results of numerical modeling of the formation and propagation of vortex structures generated by a pulsed turbulent buoyant jet have been presented for the Reynolds number Re = $1.5 \cdot 10^4$, the parameter $P = 3.65$, and the Grashof number Gr = $3.9 \cdot 10^5$. A three-dimensional turbulent flow model based on the unsteady Reynolds equations was adopted. The angle α between the jet and gravity directions was varied from 0° to 180°. The turbulent puff movement was tracked up to the moment when the maximum velocity value in the puff became equal to 3.5% of the inlet velocity. For various α values, the power-law relationships describing the propagation of the turbulent puff and a decrease in the maximum velocity value and temperature within the puff were obtained.

Keywords: mixed convection, turbulent puff, pulsed jet, numerical simulation

Funding: The reported study was funded by Russian Science Foundation (Grant No. 24-19-00437).

Citation: Ermakova K. K., Zasimova M. A., Ivanov N. G., Study of vortex flows generated by a pulsed turbulent buoyant jet, St. Petersburg State Polytechnical University Journal. Physics and Mathematics. 19 (2) (2026) 16–26. DOI: https://doi.org/10.18721/JPM.19202

This is an open access article under the CC BY-NC 4.0 license (https://creativecommons.org/licenses/by-nc/4.0/)

Научная статья
УДК 532.517
DOI: https://doi.org/10.18721/JPM.19202

ИССЛЕДОВАНИЕ ВИХРЕВЫХ ТЕЧЕНИЙ, СФОРМИРОВАННЫХ ИМПУЛЬСНОЙ ТУРБУЛЕНТНОЙ ПЛАВУЧЕЙ СТРУЕЙ

К. К. Ермакова, М. А. Засимова, Н. Г. Иванов✉

Санкт-Петербургский политехнический университет Петра Великого,
Санкт-Петербург, Россия

✉ ivanov_ng@spbstu.ru

Аннотация. Представлены результаты численного моделирования распространения вихревых облаков, сформированных импульсной турбулентной плавучей струей, для числа Рейнольдса Re = $1{,}5 \cdot 10^4$, параметра $P = 3{,}65$ и числа Грасгофа Gr = $3{,}9 \cdot 10^5$. Была принята модель трехмерного турбулентного течения, описываемого нестационарными уравнениями Рейнольдса. Угол между направлениями подачи струи и гравитационной силы α варьировался в диапазоне от 0° до 180°. Движение вихревого облака прослеживалось вплоть до момента, когда максимальное значение скорости в облаке становилось равным 3,5% от входной скорости. Для различных значений α получены степенные зависимости, описывающие распространение вихревого облака

© Ermakova K. K., Zasimova M. A., Ivanov N. G., 2026. Published by Peter the Great St. Petersburg Polytechnic University.

вдоль направления подачи струи и падение максимальной скорости и температуры в облаке.

Ключевые слова: смешанная конвекция, вихревое облако, импульсная струя, численное моделирование

Финансирование: Исследование выполнено при финансовой поддержке Российского научного фонда (грант № 24-19-00437).

Ссылка для цитирования: Ермакова К. К., Засимова М. А., Иванов Н. Г. Исследование вихревых течений, сформированных импульсной турбулентной плавучей струей // Научно-технические ведомости СПбГПУ. Физико-математические науки. 2026. Т. 19. № 2. С. 16–26. DOI: https://doi.org/10.18721/JPM.19202

Статья открытого доступа, распространяемая по лицензии CC BY-NC 4.0 (https://creativecommons.org/licenses/by-nc/4.0/)

Introduction

Turbulent jet flows are common in nature and in engineering, arising when a liquid or gas is discharged through an opening due to an applied pressure difference. The dynamics of turbulent jets have been studied experimentally and theoretically for many years [1, 2]. The findings are essential for a wide range of applications, including the design of ventilation systems, where supply jets govern air distribution, heat distribution, humidity, and contaminant concentration [3]. Heat sources also affect air distribution in practical scenarios of indoor ventilation; in some cases, their effect is comparable to that of the supplied air, and free convection develops under their influence [4].

Air in indoor ventilation systems is typically supplied at a constant flow rate. Most studies of ventilation flows have focused on the behavior of turbulent jets under steady inlet conditions. As requirements for air quality and thermal comfort become more stringent, new technical solutions are proposed. One such solution is to supply air at a variable flow rate, either gradual or intermittent. It is assumed that unsteady air supply could improve ventilation efficiency under certain conditions [5]. The effects of unsteady mechanisms for air supply are discussed in detail in the review [6], summarizing the available studies and technical solutions and concluding that the fundamentals of unsteady ventilation require further investigation.

This paper addresses a model problem of a single pulsed discharge of fluid into a quiescent environment. The vortex ring [7–9] is one of the best-known flows produced by a pulsed discharge. In addition to vortex rings, pulsed discharges can generate puffs and unsteady jets, depending on the duration and velocity of the discharge. According to [8], the vortex structures formed by a pulsed jet are characterized by the dimensionless parameter

$$P = (L_0/d)^{1/3},$$

where d is the diameter of the orifice through which the jet is supplied, L_0 is the piston stroke length ($L_0 = V_0 t_0$), t_0, V_0 are the duration and the velocity of the jet discharge.

The parameter P can be interpreted as a characteristic length of the volume added by the pulsed jet to the ambient environment, divided by the orifice diameter. Turbulent puffs (or turbulent vortex clouds) form at $1.6 < P < 8$. Vortex rings appear at smaller P; unsteady jets develop at larger values.

Experimental modeling of turbulent puffs [10, 11] was based on a technique involving repeated pulsed discharges and ensemble averaging of the monitored puff parameters. This approach has made it possible to establish several important self-similar properties of turbulent puff propagation over time, predicted theoretically in [7].

A numerical study in [12] considered the formation and motion of turbulent puffs under isothermal conditions, using an axisymmetric formulation. The study showed that the flow during a pulsed jet discharge can be divided into two phases: an initial phase, including jet discharge and puff formation, and a subsequent self-similar phase, where the velocity profiles within the fully

© Ермакова К. К., Засимова М. А., Иванов Н. Г., 2026. Издатель: Санкт-Петербургский политехнический университет Петра Великого.

developed puff remain similar to each other at successive time points. The durations of these phases were determined. Later, numerical simulation of a pulsed gas–droplet jet in an axisymmetric formulation was carried out in [13], finding that the flow structure resembled that of single-phase flow for the range of governing parameters considered.

The experiments reported in [10] examined in detail the motion of vortex structures at a distance from the discharge source (the self-similar phase). The position of the turbulent puff was found to follow a power-law dependence for isothermal conditions: At^B, where $B = 0.25$. The puff velocity also varied over time following a power-law dependence, with an exponent $B = -0.75$. The parametric simulations in [12] were also approximated by these power-law dependences.

Unlike [12], our paper reports on numerical simulations of non-isothermal flow generated by a single pulsed buoyant jet discharged into a quiescent environment. We carried out a parametric investigation into the influence of the angle between the jet direction and the gravity vector on the structure of the resulting vortex flow.

Problem statement and computational procedure

Similar to the problem statement in our earlier paper [12], here we consider the flow of an incompressible fluid (air) in a half-space bounded by an impermeable solid wall (Fig. 1); however, the problem is now treated as three-dimensional.

Circular orifice *1* of diameter d (set to $d = 0.05$ m in the dimensional formulation) is located on the wall; a pulsed air jet is discharged through it normal to solid surface *2*. The coordinate origin is located at the orifice center, with the z-axis directed into the domain normal to the bounding wall. The flow is assumed symmetric with respect to the mid-plane of the inlet orifice, so a symmetry condition is applied at the boundary *3* ($x = 0$). The remaining boundaries of the computational domain (*4*) are open (permeable). The dimensions of the computational domain are $24d \times 101d \times 120d$.

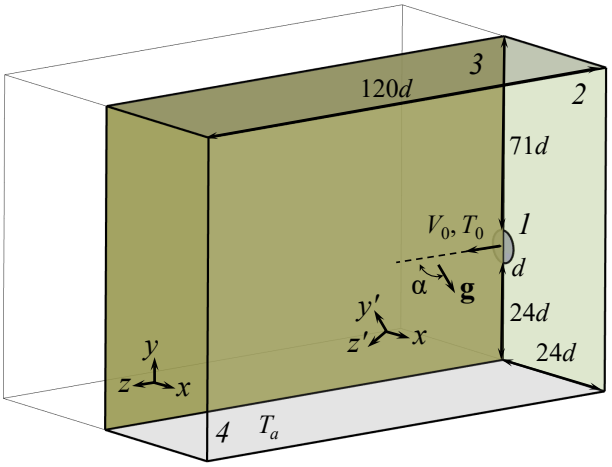


Fig. 1. Schematic diagram of computational domain: inlet orifice *1*, wall *2*, symmetry plane *3*, permeable boundary *4*;
d is the diameter of the inlet orifice; α is the angle between the jet direction and the gravity vector; the values of the parameters V_0, T_0, T_a and α are given in the text; **g** is the gravitational acceleration

The fluid is at rest at the initial time $t = 0$, and its temperature T_a is assumed uniform. During the period $0 \le t \le t_0$, fluid is discharged through the orifice at a constant velocity V_0 and temperature T_0. The following parameter values were adopted for simulations in the dimensional formulation:

$$V_0 = 4.28 \text{ m/s}, \; t_0 = 0.57 \text{ s},$$
$$\Delta T = T_0 - T_a = 20 \text{ K}, \; T_a = 293 \text{ K}.$$

Buoyancy effects were taken into account in the Boussinesq approximation: the value of $\beta \Delta T$ (β is the thermal expansion coefficient) is less than 0.07. The angle α between the jet direction and the gravity vector (see Fig. 1) was varied from 0° to 180° (at α = 0°, the jet was discharged in the direction of the gravity vector). Additional coordinate axes (x', y', z') were introduced for further data processing, with $x' = x$, and the y'-axis directed opposite to the gravity vector.

The problem is governed by three dimensionless parameters:

$$\text{Reynolds number Re} = V_0 d/\nu = 10 \cdot 1.5^4,$$
$$\text{parameter } P = (V_0 t_0/d)^{1/3} = 3.65,$$
$$\text{Grashof number Gr} = g\beta d^3 \Delta T/\nu^2 = 10 \cdot 3.9^5.$$

Note that these parameters were determined from the values of the quantities during the discharge phase. At this stage, the Richardson number $\mathrm{Ri} = Gr/Re^2$ was much less than unity, indicating predominantly forced convection. In later phases, as the characteristic velocity of the turbulent puff decreased, Ri values approached unity.

The simulations were run with a quasi-structured computational mesh containing 540,000 cells. An *O*-type grid topology was used for spatial discretization, with refinement near the orifice along both radial and axial directions; 44 cells were placed along the circumferential direction of the orifice and 22 along the radial direction. A mesh sensitivity study was carried out, showing that doubling the number of cells in each direction only slightly changed the characteristics of the vortex structures, so the solution obtained with the base mesh was assumed to be mesh-independent.

The problem was solved numerically in the ANSYS Fluent CFD package; the computational resources of the Polytechnic Supercomputer Center (scc.spbstu.ru) were used. Unsteady turbulent flow and heat transfer were simulated by solving the unsteady Reynolds-averaged Navier–Stokes (URANS) equations. The standard k–ε turbulence model was applied for closure. Constant values of turbulent viscosity ($\nu_{t0}/\nu = 10$) and turbulence intensity ($I_0 = 5\%$) were set at the inlet; these were converted into inlet values of k and ε in the code. These conditions correspond to a moderate turbulence level near the orifice. The turbulent Prandtl number was set to 0.9. Second-order spatial and temporal discretization schemes were used. The time step was $0.086V_0/d$. The total simulation time was about 3,000 convective time units $t' = tV_0/d$.

Motion and parameters of the turbulent puff

The motion of the vortex structure generated by the pulsed jet is illustrated for the case with an angle between the jet direction and the gravity vector $\alpha = 120°$. The flow structure resembled that described in [10] during the initial phase of puff formation and propagation (for $t' < 80$), due to the predominant role of forced convection. The contribution of natural convection becomes noticeable for $t' > 80$. Accordingly, analysis of the flow structure in this paper focuses on the main phase in the propagation of the turbulent puff, after the puff has fully developed.

Fig. 2 shows the fields of velocity magnitude, vorticity magnitude, and temperature at three points in time after the start of the pulsed jet discharge: $t' = 86$, 600, and 2910. The velocity values are normalized by the maximum velocity magnitude at each time point, $|\mathbf{V}_c|$. The center of the puff is taken as the point C $(0, y_c, z_c)$, where the velocity magnitude reaches its maximum at that time. The vorticity magnitudes are normalized by the maximum vorticity at that time, $\Omega_{\max}$. The temperature $\theta = (T - T_a)/(T_{\max} - T_a)$ is normalized by the difference between the maximum temperature within the puff at that time, $T_{\max}$, and the ambient temperature.

As seen from the vorticity field, the vortex structure at $t' = 86$ is elongated in the direction of jet discharge, but its shape gradually approaches a sphere (see Fig. 2,*a*). Elevated Ω values are localized in a region roughly $8d \times 8d \times 10d$ in size. The center of the puff only slightly deviates from the jet axis (it is at a distance less than d from the axis). By this point in time, the maximum velocity has dropped by about 75% relative to the discharge velocity V_0, and the temperature difference $(T_{\max} - T_a)$ has dropped by 78% relative to the initial difference $(T_0 - T_a)$.

At $t' = 600$, the characteristic dimensions of the puff grow to about $15d \times 15d \times 15d$, while the puff noticeably deviates from the initial direction: the velocity maximum is located at about $5d$ from the jet axis (see Fig. 2,*b*). The vorticity fields are asymmetric relative to the center of the vortex structure: the values in the lower part of the puff are larger than in the upper part. By this time, the strength of the puff is considerably weakened: the maximum of the velocity magnitude $|\mathbf{V}_c|$ is about 5% of the velocity V_0, and the temperature difference is less than 3% of the initial value.

By the time $t' = 2910$, the dimensions of the puff increase by roughly another factor of two in each direction, reaching about $30d \times 30d \times 30d$ (see Fig. 2,*c*). The flow activity continues to decay: the streamwise and cross-stream velocity components are comparable and do not exceed 2% of the inlet velocity. A thermal wake trailing behind the puff can be seen in the fields, moving even more slowly and essentially separated from the puff.

We should note that further evolution of the puff up until it stops completely cannot be reliably simulated by the URANS approach; eddy-resolving methods would be required to simulate the decay phase of turbulent flow, which is beyond the scope of this paper.

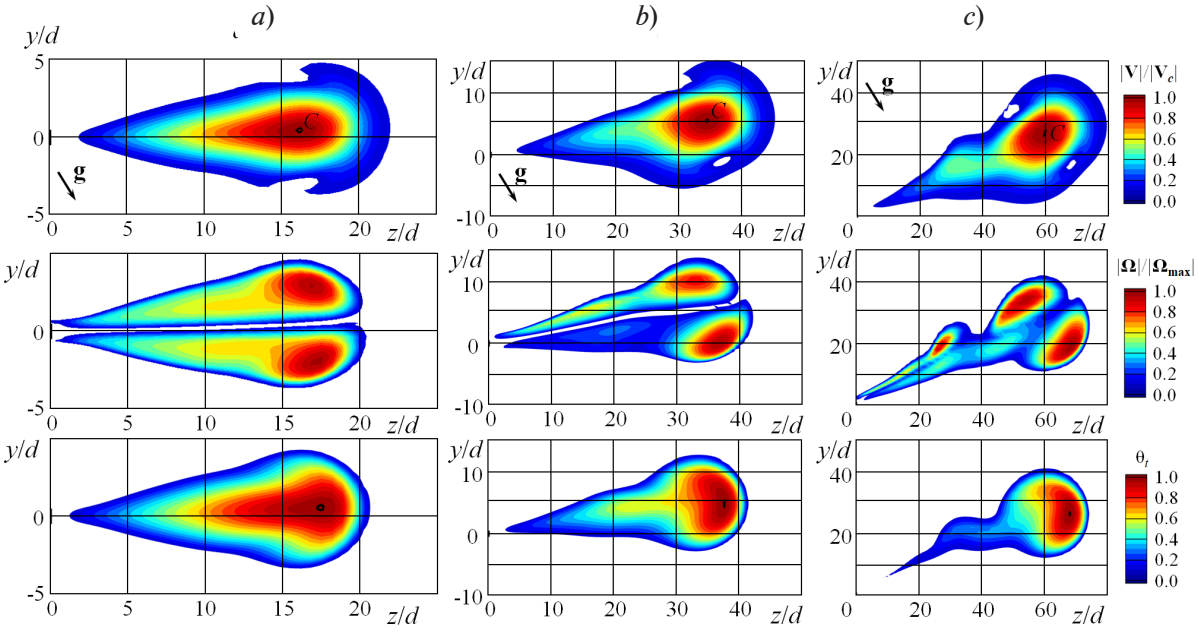


Fig. 2. Calculated fields of velocity magnitude (top row), vorticity magnitude (middle row), and temperature (bottom row) at three time points t': 86 (*a*), 600 (*b*), and 2910 (*c*). Case $\alpha = 120°$

Fig. 3 shows the evolution of the puff position over time and in space. Observation of the puff center position (solid line) starts when the center is located about three orifice diameters ($3d$) from the inlet orifice ($t' \approx 50$). After the puff is fully formed, when the point z_c has moved rapidly away from the source (at $t' > 100$), the trajectory curve of the puff center (see Fig. 3,*a*, the dependence $y_c(z_c)$) begins to deviate from the jet direction; the function $y_c(z_c)$ is close to cubic up to t' values on the order of 10^3.

The dependence $z_c(t)$ follows a power law with an exponent of 0.35 in the interval $100 < t' < 1000$; notably, the exponent in the self-similar phase should be equal to 0.25 for the propagation of an isothermal puff (according to [10]). Some deviation from these power-law dependences is observed for larger t' ($t' > 1000$), i.e., during the slow decay phase (low drift velocity). The puff center deviates substantially over the simulation period: the final position (the fields shown in Fig. 2,*c*) corresponds to the point (0, $27d$, $60d$).

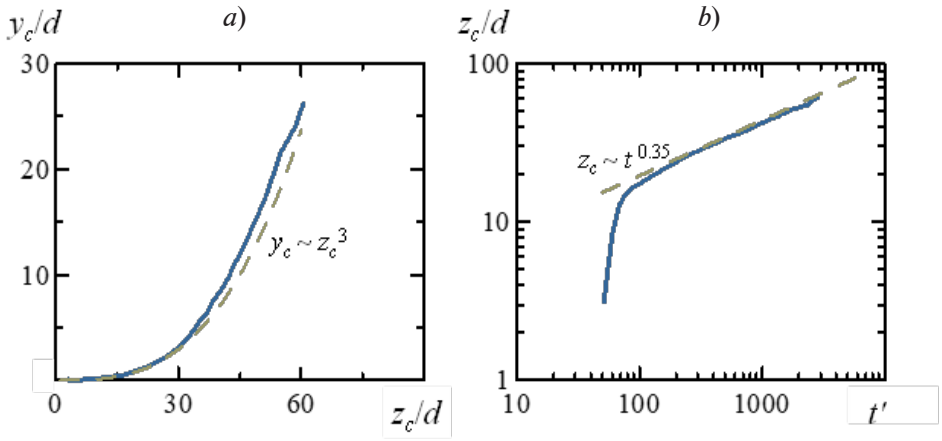


Fig. 3. Evolution of the position in maximum of vortex cloud velocity in space (*a*) and over time (*b*). Dashed lines mark the approximating functions

Fig. 4 shows the evolution of the maximum velocity magnitude $|\mathbf{V}_c|(t)$, as well as its streamwise ($V_{c,z}(t)$) and cross-stream ($V_{c,y}(t)$) components. The dashed lines in Fig. 4,*a* characterize the variation of $|\mathbf{V}_c|(t)$ following the power-law dependences with exponents of −0.75 and −0.40. Unlike the isothermal case [10], where the behavior of $V_c(t)$ in the self-similar phase follows a power-law dependence with a fixed exponent of −0.75, this behavior is only observed for the pulsed buoyant jet in the interval $100 < t' < 600$, when the streamwise velocity is much larger than the cross-stream component (see Fig. 4,*b*). The values of $V_{c,z}(t)$ and $V_{c,y}(t)$ approach each other at larger t', and the curve of the maximum velocity magnitude $|\mathbf{V}_c|(t)$ deviates from the earlier trend, following a new power-law dependence with an exponent of −0.4.

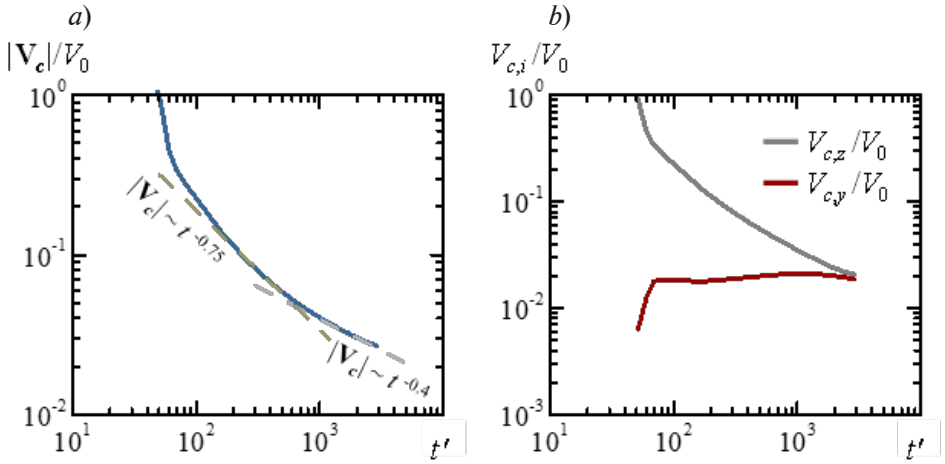


Fig. 4. Time evolution computed for maximum velocity magnitude of vortex cloud (*a*); its streamwise and cross-stream components (*b*)

Fig. 5 characterizes the time evolution of the characteristic temperature within the puff, showing the data for the normalized maximum temperature

$$\theta_{\max} = (T_{\max} - T_a)/(T_0 - T_a),$$

i.e., the temperature difference (normalized by the initial difference $T_0 - T_a$) between the instantaneous maximum temperature in the puff and the ambient temperature T_a.

Over the time interval considered, the dependence $\theta_{\max}(t)$ follows a power law with an exponent of −1.03. At $t' \approx 1400$, the maximum temperature difference $T_{\max} - T_a$ amounts to 1% of the initial value of $T_0 - T_a$.

The maximum velocity magnitude in the puff decreased less dramatically, to 3.5% of the jet velocity. It is worth repeating that analysis of further propagation of the puff, with predominant natural convection, lies beyond the scope of this paper.

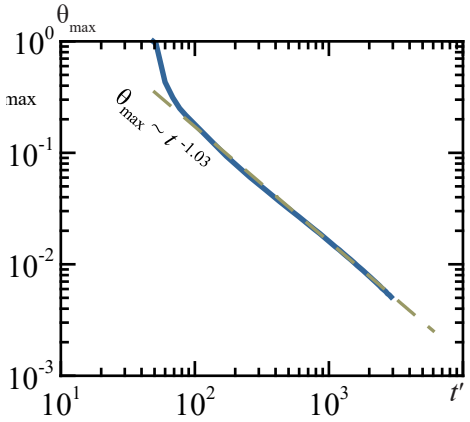


Fig. 5. Time evolution of maximum temperature in the vortex cloud
The dashed line marks the approximation of a segment of the dependence by a power-law function

Propagation of the puff as a function of pulsed jet direction

This section presents the results of parametric simulations for 7 cases that differ in the angle α between the jet direction and the gravity vector (the angle α was varied from 0° to 180° in steps of 30°). For each case, we considered time samples up to $t' < t'_{3.5\%}$, where $t'_{3.5\%}$ is the time when the maximum velocity magnitude $|\mathbf{V}_c|$ drops to 3.5% of the inlet velocity. Depending on the case, $t'_{3.5\%}$ ranged from 340 (α = 0°) to $2 \cdot 10^3$ (α = °180). Fig. 6,*a* shows the trajectories of the puff centers for all seven cases (curves characterizing the deviation in the position of the velocity maximum) in coordinates (x, y', z'); Fig. 6,*b* shows the distributions of velocity magnitude at the final time point in the sample, $t' = t'_{3.5\%}$. Evidently, the puff propagates along the jet axis for α = 0° and 180°; the puff deviates from this axis under the action of buoyancy forces for the other values of α. As the angle α increases, the length of the trajectory traveled by the puff up to a given decay level gradually increases, and so does the size of the puff (see Fig. 6,*b*).

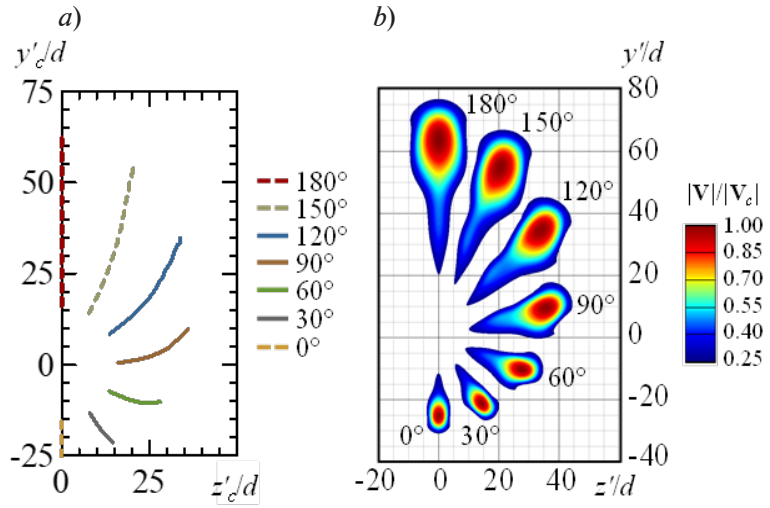


Fig. 6. Parametric simulations for different angles α: cloud center trajectories (*a*); distributions of velocity magnitude a $t' = t'_{3.5\%}$(*b*) (see text for details)

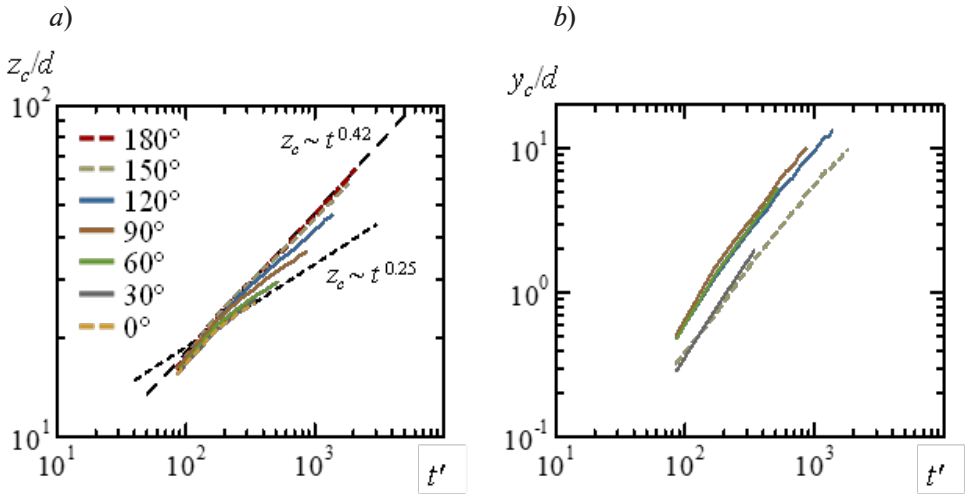


Fig. 7. Time evolution computed for the position of vortex cloud center for cases with different α (angle between the jet and gravity directions)

Fig. 7 shows the time evolution in the position of the puff center for the seven computational cases (the graphs are plotted in coordinates aligned with the jet direction). The family of curves $z_c(t)$, describing puff propagation along the jet direction, is supplemented by two dashed lines approximating the limiting power-law dependences (see Fig. 7,*a*). For $\alpha = 0°$, when the jet is discharged in the direction of gravity, the calculated data are approximated by a power-law dependence with an exponent of 0.25, which corresponds to the isothermal case [12]. In the opposite limiting case, when the pulsed jet is discharged upward and gravity accelerates it ($\alpha = 180°$), the computational data are approximated by a power-law dependence with an exponent of 0.42. Distinct stratification can be observed in the curves $y_c(t)$ in Fig. 7,*b*, characterizing the deviation of the puff from the jet direction: the largest deviation occurs when the jet is discharged perpendicular to the gravity vector ($\alpha = 90°$). The plots for $\alpha = 60°$ and 120°, describing the gradual deviation of the puff center, lie slightly below this curve. The difference between the curves plotted from the data for $\alpha = 30°$ and 150° is more pronounced: in these cases, the puff drifts away from the axis more slowly.

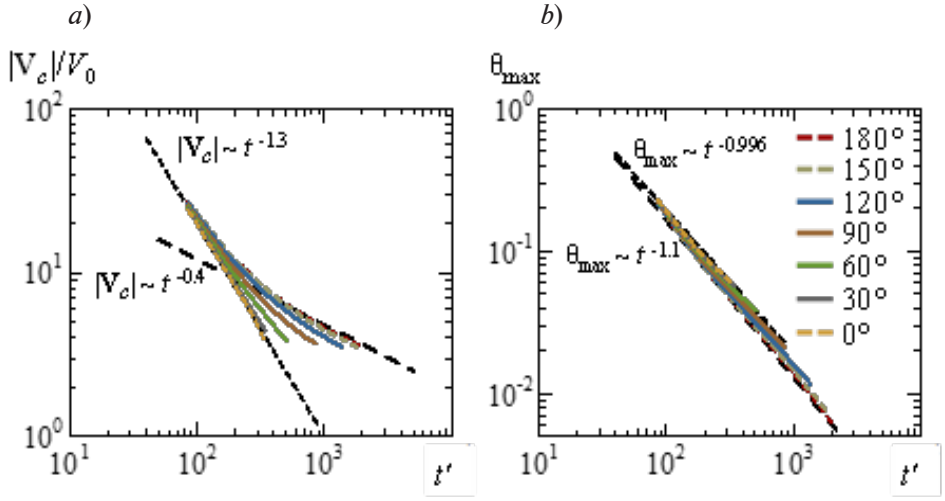


Fig. 8. Time evolution of normalized maximum velocity (*a*) and normalized maximum temperature (*b*) for cases with different angles α
The dashed lines mark power-law approximations for the limiting cases ($\alpha = 0°$ and $\alpha = 180°$)

Fig. 8 shows the curves characterizing the decay of the maximum velocity and normalized maximum temperature over time. As in Fig. 7,*a*, the families of curves are supplemented by dashed lines approximating the limiting power-law dependences (for $\alpha = 0°$ and $\alpha = 180°$). The puff decelerates most rapidly for $\alpha = 0°$, which is unsurprising: buoyancy exerts a significant braking effect. The evolution of $V_c(t)$ in this case follows a power-law dependence with an exponent of −1.3. In contrast, buoyancy weakens the deceleration of the puff for $\alpha = 180°$, and $V_c(t)$ decays over time with an exponent of −0.4. The differences in the decay of the characteristic puff temperature between the cases are less pronounced: all curves lie close to each other, and the exponents range from −0.996 for $\alpha = 0°$ to −1.100 for $\alpha = 180°$.

Conclusion

This study reports on the results from three-dimensional URANS simulations of non-isothermal flow generated by a single pulsed buoyant jet discharged into a quiescent environment. Forced convection dominated during the initial phase of turbulent puff formation and propagation, which lasted for less than 100 dimensionless time units. Natural convection made a substantial contribution at longer times.

Analysis of the flow structure focused on the main phase of puff propagation continuing up to the time when the maximum velocity magnitude $|\mathbf{V}_c|$ dropped to 3.5% of its inlet value.

Parametric simulations where the angle α between the jet and gravity directions was varied from 0° to 180° showed that the discharge direction of the pulsed buoyant jet strongly affects both the propagation trajectory of the puff and its decay rate. The dependence describing the

propagation of the puff along the jet direction follows a power law, with the exponent ranging from 0.25 (corresponding to the isothermal case) to 0.42, depending on the discharge direction.

The decrease in the maximum velocity within the puff over time is also approximated by a power law, with exponents between −1.3 and −0.4.

The decrease in the characteristic temperature within the puff is less sensitive to α (the angle between the jet and the gravity directions): the exponent is close to −1 for all cases considered.

Future research will focus on the behavior of vortex structures at different values of the parameter *P*, in particular, adopting scale-resolving simulation approaches.

REFERENCES

1. **Abramovich G. N., Girshovich T. A., Krasheninnikov S. Iu., et al.,** The theory of turbulent jets, Ed. by G. N. Abramovich, 2-nd ed., Nauka Publishing, Moscow, 1984 (in Russian).

2. **List E. J.,** Turbulent jets and plumes, Ann. Rev. Fluid Mech. 14 (Jan) (1982) 189–212.

3. **Grimitlin M. I.,** Raspredeleniye vozdukha v pomeshcheniyakh [Indoor air distribution], Published by AVOK Severo-Zapad [Ventilation, Heating, air Conditioning Association (VHCA) of engineers in the North-West], Saint-Petersburg, 2004 (in Russian).

4. **Davies Wykes M. S., Chahour E., Linden P.F.,** The effect of an indoor-outdoor temperature difference on transient cross-ventilation, Build. Environ. 168 (15 Jan) (2020) 10644.

5. **Fan M., Fu Z., Wang J., et al.,** A review of different ventilation modes on thermal comfort, air quality and virus spread control, Build. Environ. 212 (15 March) (2022) 108831.

6. **Mesenhöller E., Vennemann P., Hussong J.,** Unsteady room ventilation – A review, Build. Environ. 2020. Vol. 169 (Febr) (2020) 106595.

7. **Glezer A., Coles D.,** An experimental study of a turbulent vortex ring, J. Fluid Mech. 211 (Febr) (1990) 243–283.

8. **Shariff K., Leonard A.,** Vortex rings, Ann. Rev. Fluid Mech. 24 (Jan) (1992) 235–279.

9. **Akhmetov D. G.,** Vortex rings, Springer-Verlag, Berlin, Heidelberg, 2009.

10. **Sangras R., Kwon O. C., Faeth G. M.,** Self-preserving properties of unsteady round nonbuoyant turbulent starting jets and puffs in still fluids, ASME. J. Heat Transfer. 124 (3) (2002) 460–469.

11. **Ghaem-Maghami E., Johari H.**, Concentration field measurements within isolated turbulent puffs, ASME. J. Fluids Eng. 129 (2) (2007) 194–199.

12. **Zasimova M. A., Ris V. V., Ivanov N. G.,** Numerical simulation of the formation and motion of turbulent vortex clouds (puffs), Fluid Dyn. 58 (5) (2023) 882–893.

13. **Pakhomov M. A., Terekhov V. P.,** Distinctive features of propagation of a turbulent pulsed gas-droplet eddy cloud. Fluid Dyn. 59 (4) (2024) 687–699.

СПИСОК ЛИТЕРАТУРЫ

1. **Абрамович Г. Н., Гиршович Т. А., Крашенинников С. Ю. и др.** Теория турбулентных струй. Под ред. Г. Н. Абрамовича. -2е изд., перераб. и доп. М.: Наука, 1984. 716 с.

2. **List E. J.** Turbulent jets and plumes // Annual Review of Fluid Mechanics. 1982. Vol. 14. January. Pp. 189–212.

3. **Гримитлин М. И.** Распределение воздуха в помещениях. Изд. 3-е, доп. и испр. СПб.: АВОК Северо-Запад, 2004. 320 с.

4. **Davies Wykes M. S., Chahour E., Linden P.F.** The effect of an indoor-outdoor temperature difference on transient cross-ventilation // Building and Environment. 2020. Vol. 168. 15 January. P. 10644.

5. **Fan M., Fu Z., Wang J., Wang Z., Suo H., Kong X., Li H.** A review of different ventilation modes on thermal comfort, air quality and virus spread control // Building and Environment. 2022. Vol. 212. 15 March. P. 108831.

6. **Mesenhöller E., Vennemann P., Hussong J.** Unsteady room ventilation – A review // Building and Environment. 2020. Vol. 169. February. P. 106595.

7. **Glezer A., Coles D.** An experimental study of a turbulent vortex ring // Journal of Fluid Mechanics. 1990. Vol. 211. February. Pp. 243–283.

8. **Shariff K., Leonard A.** Vortex rings // Annual Review of Fluid Mechanics. 1992. Vol. 24. January. Pp. 235–279.

9. **Ахметов Д. Г.** Вихревые кольца. Новосибирск: ГЕО, 2007. 151 с.

10. **Sangras R., Kwon O. C., Faeth G. M.** Self-preserving properties of unsteady round nonbuoyant turbulent starting jets and puffs in still fluids // ASME. Journal of Heat Transfer. 2002. Vol. 124. No. 3. Pp. 460–469.

11. **Ghaem-Maghami E., Johari H.** Concentration field measurements within isolated turbulent puffs // ASME. Journal of Fluids Engineering. 2007. Vol. 129. No. 2. Pp. 194–199.

12. **Засимова М. А., Рис В. В., Иванов Н. Г.** Численное моделирование формирования и движения турбулентных вихревых облаков // Известия Российской академии наук. Механика жидкости и газа. 5 № .2023. С. 69–57.

13. **Пахомов М. А., Терехов В. И.** Особенности распространения газокапельного турбулентного импульсного вихревого облака // Известия Российской академии наук. Механика жидкости и газа. 2024. № 4. С. 55–68.

THE AUTHORS

ERMAKOVA Karina K.
Peter the Great St. Petersburg Polytechnic University
29 Politechnicheskaya St., St. Petersburg, 195251, Russia
karinak77777@mail.ru

ZASIMOVA Marina A.
Peter the Great St. Petersburg Polytechnic University
29 Politechnicheskaya St., St. Petersburg, 195251, Russia
zasimova_ma@spbstu.ru
ORCID: 0000-0002-4103-6574

IVANOV Nikolay G.
Peter the Great St. Petersburg Polytechnic University
29 Politechnicheskaya St., St. Petersburg, 195251, Russia
ivanov_ng@spbstu.ru
ORCID: 0000-0001-9897-5401

СВЕДЕНИЯ ОБ АВТОРАХ

ЕРМАКОВА Карина Константиновна – *студентка Физико-механического института Санкт-Петербургского политехнического университета Петра Великого.*
195251, Россия, г. Санкт-Петербург, Политехническая ул., 29
karinak77777@mail.ru

ЗАСИМОВА Марина Александровна – *кандидат физико-математических наук, доцент Высшей школы прикладной математики и вычислительной физики Санкт-Петербургского политехнического университета Петра Великого.*
195251, Россия, г. Санкт-Петербург, Политехническая ул., 29
zasimova_ma@spbstu.ru
ORCID: 0000-0002-4103-6574

ИВАНОВ Николай Георгиевич – *кандидат физико-математических наук, заведующий научно-исследовательской лабораторией гидродинамики, директор Физико-механического института Санкт-Петербургского политехнического университета Петра Великого.*
195251, Россия, г. Санкт-Петербург, Политехническая ул., 29
ivanov_ng@spbstu.ru
ORCID: 0000-0001-9897-5401

Received 27.11.2025. Approved after reviewing 08.12.2025. Accepted 08.12.2025.
Статья поступила в редакцию 27.11.2025. Одобрена после рецензирования 08.12.2025. Принята 08.12.2025.

© Peter the Great St. Petersburg Polytechnic University, 2026